



Performance enhancement of atmospheric turbulence channels in DWDM-FSO PON communication systems using M-ary hybrid DPPM-M-PAPM modulation schemes under pointing errors, ASE noise and interchannel crosstalk

Ebrahim E. Elsayed¹

Received: 26 April 2024 / Accepted: 10 May 2024

© The Author(s), under exclusive licence to The Optical Society of India 2024

Abstract This paper focuses on improving the efficiency of free-space optical (FSO) communication by employing a combination of hybrid on-off keying (OOK) modulation, M-ary digital pulse position modulation (M-ary DPPM), and M-pulse amplitude and position modulation (M-PAPM). The study aims to analyze and enhance the bit-error-rate (BER) performance using techniques such as the moment generating function, modified Chernoff bound, and Gaussian approximation, while taking into account challenges like amplified spontaneous emission (ASE) noise, atmospheric turbulence (AT), pointing errors (PEs), and interchannel crosstalk (ICC). The proposed system model revolves around a passive optical network (PON) that utilizes wavelength division multiplexing (WDM) for dense WDM (DWDM), with a focus on the hybrid fiber FSO (HFFSO) link. By utilizing eight wavelength channels transmitting at a rate of 2.5 Gbps over a turbulent HFFSO-DWDM system and PON-FSO optical fiber, starting at a 1550 nm channel spacing in the C-band of 100 GHz, the research demonstrates successful 20 Gbit/s–4000 m transmission with promising results. To enhance performance, the modulation technique of M-ary DPPM-M-PAPM is used to provide additional information bits. The integration of adaptive optics is also suggested to mitigate the effects of atmospheric turbulence and improve modulation efficiency. The study reveals that the proposed M-ary hybrid DPPM-M-PAPM solution increases receiver sensitivity compared to OOK, ensuring reliability and achieving a lower power penalty of 0.2–3.0 dB at a low

coding level (M) of 2 in WDM-FSO systems under weak turbulence conditions. The hybrid OOK/M-ary DPPM-M-PAPM modulation scheme offers an optical signal-to-noise ratio ranging from 4 to 8 dB in the DWDM-HFFSO link under conditions of strong turbulence, aiming for a target BER of 10^{-12} . Numerical findings suggest that this approach can be further optimized by combining hybrid OOK/M-DPPM and M-PAPM for DWDM-HFFSO systems. Calculations indicate that PAPM-DPPM outperforms OOK non-return-to-zero (NRZ) by approximately 10 dB to 11 dB at a BER of 10^{-12} . Incorporating an aperture diameter of 10 cm and an average transmitted optical power of 13 dBm, along with aperture averaging, M-ary hybrid DPPM-M-PAPM, and spatial diversity, results in the average spectral efficiency performance at 53 bit/s/Hz and 38 bit/s/Hz without and with PEs, respectively. Utilizing a coding level of 5 and aiming for a BER of 10^{-12} , M-ary DPPM-M-PAPM offers about a 9 dB sensitivity improvement over the OOK-NRZ FSO system. Achieving a BER target of 10^{-12} , DPPM enhances sensitivity by approximately 10–11 dB compared to DWDM-FSO OOK-NRZ. Simulation results affirm the viability of the proposed hybrid optical modulation technique for DWDM-FSO hybrid links in both optical-wireless and fiber-optic communication systems, significantly enhancing their overall efficiency. To further improve performance, the paper suggests the integration of adaptive optics to mitigate the effects of atmospheric turbulence and enhance modulation efficiency. The proposed M-ary hybrid DPPM-M-PAPM solution contributes to increased sensitivity and lower power penalty, particularly at low coding levels, demonstrating its potential for DWDM-FSO systems. Numerical findings suggest that this approach can be further optimized for enhanced spectral efficiency and sensitivity over traditional modulation schemes. By leveraging the M-ary DPPM-M-PAPM modulation technique and adaptive

✉ Ebrahim E. Elsayed
engebrahim16@std.mans.edu.eg; engebrahim16@gmail.com

¹ Department of Electronics and Communication Engineering, Faculty of Engineering, Mansoura University, Mansoura 35516, El-Dakahilia, Egypt

optics, the study demonstrates improved receiver sensitivity compared to traditional OOK modulation, ensuring robust performance under varying atmospheric conditions. Numerical findings indicate significant enhancements in system performance metrics, offering a promising solution for optimizing DWDM-FSO communication systems in challenging environments. Finally, the adoption of hybrid OOK/M-ary DPPM-M-PAPM modulation schemes represents a novel strategy for mitigating effects of AT, PEs, ASE, and ICC in DWDM-FSO optical fiber communication systems.

Keywords DWDM-FSO/PON optical fiber network communication systems · hybrid OOK/M-ary DPPM-M-PAPM · ASE noise · Interchannel crosstalk (ICC) · Modified Chernoff bound · Pointing errors (PEs)

Introduction

The modulation schemes, such as Pulse Position Modulation (PPM) and Digital PPM (DPPM), showcase exceptional performance capabilities in various settings, including free-space optical (FSO) transmission links [1, 2]. These schemes are widely applied in diverse scenarios like FSO links, hybrid fibers, optical wireless communication (OWC), subsequent FSO systems, satellite-to-satellite connections, atmospheric turbulence (AT), interchannel crosstalk (ICC), and indoor wireless channels [1–3]. DPPM modulation boosts power efficiency without the necessity of continuous monitoring of decision-making circuit thresholds [4, 5]. Extensive experimentation has been conducted on hybrid fiber/FSO (HFFSO) systems and OWC platforms [5–9], with research indicating that DPPM and PPM schemes surpass on–off keying (OOK) in terms of sensitivity and power efficiency in the HFFSO link. The exploration of M-pulse amplitude and position modulation (M-PAPM) for both pulse amplitude modulation (PAM) and PPM has been crucial in the realm of optical fiber (OF) communications [5–8]. M-PAPM excels in delivering high efficiency and sensitivity in FSO communication due to its dispersion-free nature [1, 5, 8]. To accommodate the escalating bandwidth demands for higher data rates in OF, AT, OWC, and indoor networks [8–15], suggestions have been made to implement wavelength division multiplexing (WDM) techniques and dense WDM (DWDM) systems. The integration of WDM technology in HFFSO, OWC, and hybrid OF/multiple networks holds promise in crafting high-performance systems with solutions for bandwidth optimization, capable of long-range transmission, higher bit rates, advanced technology, and enhanced data security for WDM passive optical networks (WDM-PON) [8, 9, 13, 16]. The research presented in this paper delves into the enhancement of free-space optical communication systems

by implementing a novel approach combining hybrid OOK modulation, M-ary digital pulse position modulation (M-ary DPPM), and M-PAPM. The primary objective is to improve the bit-error-rate (BER) performance considering challenges like amplified spontaneous emission (ASE) noise, AT, pointing errors (PEs), and ICC. By utilizing innovative techniques such as the moment generating function, modified Chernoff bound, and Gaussian approximation, the study aims to boost system efficiency and reliability in DWDM-FSO PON communication systems. The use of techniques such as moment generating functions (MGF), Chernoff bound (CB), Gaussian approximations (GA), and modified Chernoff bound (MCB) has been pivotal in addressing ASE in FSO transmission links and establishing upper limits on BER [5, 8, 9, 17–20]. Furthermore, the incorporation of adaptive optics (AO) and compensation techniques has been recommended to mitigate the impact of AT and enhance system performance [17]. The principal contributions outlined in the research encompass the utilization of M-ary DPPM-M-PAPM modulation to enhance efficiency by delivering additional bits, integrating AO to diminish ICC interferences and bolster reliability, achieving favorable BER outcomes with reduced complexity, providing theoretical BER expressions and simulation results for M-DPPM-M-PAPM modulation schemes in WDM-PON/HFFSO scenarios, and proposing hybrid OOK/M-ary DPPM-M-PAPM and AO strategies to enhance performance and efficiency in receivers of WDM-HFFSO systems through OOK non-return-to-zero (OOK-NRZ) modulation. By concentrating on improving power penalty (PP) performance and system efficiency for WDM-HFFSO systems, optical-wireless networks, and fiber-optic communication systems, the study aims to deliver substantial advancements. The research enhances hybrid OOK/DPPM-M-PAPM techniques to boost signal-to-noise ratios (SNRs) in HFFSO systems amid AT effects, ICC, and ASE. This enhancement is outlined in prior works [9] (<http://eprints.nottingham.ac.uk/13304/1/AladelobaAbisayoThesis.pdf>). We make the following contributions to this research. This methodology encompasses key aspects such as: (1) **Advancement in Modulation Techniques:** The paper introduces hybrid modulation approaches combining M-ary DPPM-M-PAPM. This novel combination aims to enhance BER performance, crucial for improving the reliability and efficiency of communication systems. (2) **Robustness Against Environmental Challenges:** The study focuses on systems operating under adverse conditions such as atmospheric turbulence, pointing errors (PEs), ASE noise, and interchannel crosstalk. These factors commonly degrade system performance, and the proposed modulation and system design aim to mitigate these effects efficiently. (3) **Realistic and Scalable System Design:** By analyzing systems under

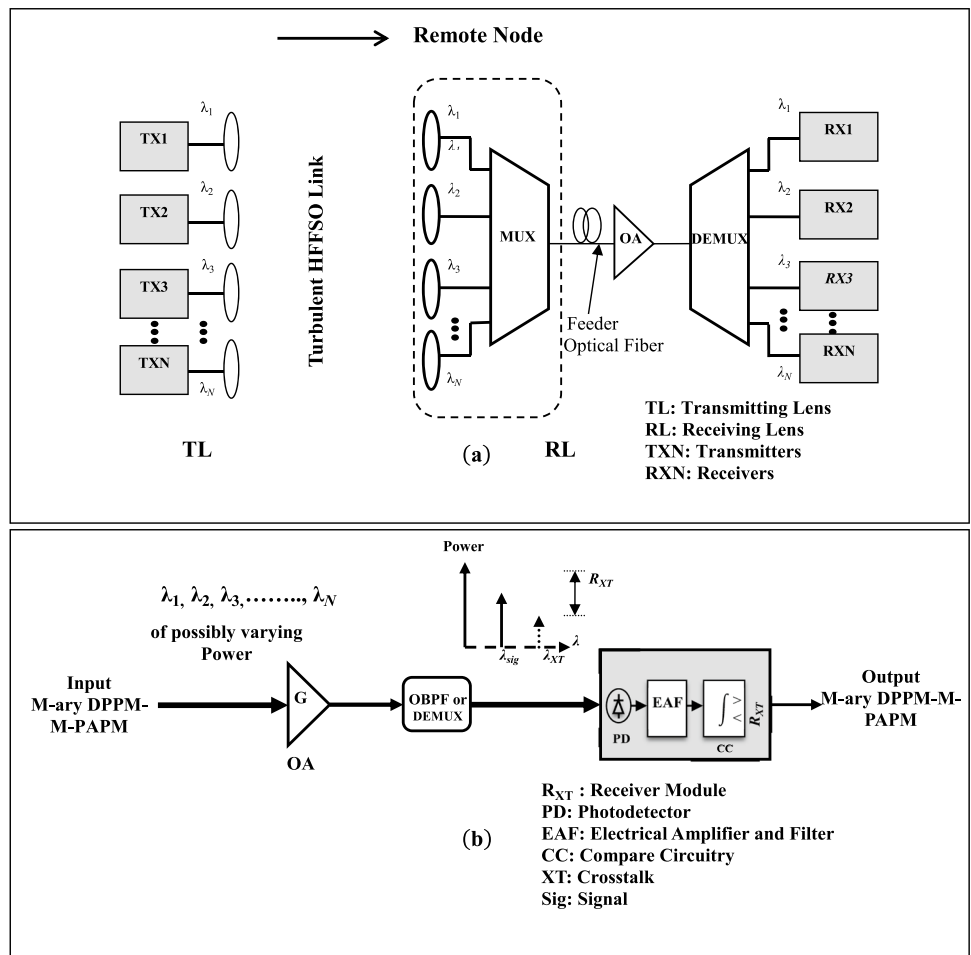
realistic environmental conditions and proposing solutions applicable to DWDM systems, this research moves towards practical, scalable solutions for real-world optical communication networks. (4) Improved System Performance: The proposed system model shows enhanced performance metrics like receiver sensitivity and reduced power penalty, important for increasing the distance and quality of FSO communications. The study further refines calculations and evaluations to mitigate AT, PE, and ASE noise. In summary, this research lays the foundation for a more efficient and reliable communication system for DWDM-FSO PON networks, addressing key challenges such as AT, PEs, ASE noise, and ICC. The proposed modulation schemes and system design hold promise in improving system performance metrics like receiver sensitivity, PP, and overall efficiency, making significant strides in the realm of optical communication networks. The paper is structured as follows: "System description" Section outlines the proposed PON/WDM-HFFSO optical fiber communication system, "M-ary hybrid DPPM-M-PAPM modulation" Section details the M-ary DPPM-M-PAPM model for the hybrid WDM-PON/HFFSO link, "Adverse atmospheric

channel" Section analyzes AT channel effects, "Results and discussions" Section presents numerical results, and "Practical implications and applications" Section draws conclusions for the study.

System description

In the system overview provided, slots of length $t_s = MT_b/n$ in DPPM frames are determined by $n = 2^M$, where $T_b = 1/R_b$ denotes the bit cycle, R_b represents the data rate, and M signifies the coding level (CL) [9]. Among the challenges faced by the HFFSO-PON systems are ASE noise (ASEN), beam-spreading, beam-absorption, attenuation, ICC, and splitting losses at the OBPF/demux for optical signals (OS) as depicted in Fig. 1a. The system, simulated using MATLAB software (2020) via Monte-Carlo simulations, utilizes eight channels of WDM-DWDM starting from 1550 nm over single-mode fiber with a 100 GHz channel spacing in the C-band of the ITU. Results showcase a 20 Gbit/s—4000 m transmission with favorable performance due to the combination of 2.5 Gbps data rate across 8 channels [21].

Fig. 1 System design for an 8-channel PON-DWDM-HFFSO accommodating OOK-NRZ/M-ary DPPM-M-PAPM in conditions of moderate turbulence (MT), strong turbulence (ST), and weak turbulence (WT): **a** presents the suggested framework for assessing ICC, while **b** depicts the receiver system schematics. This representation is adapted from [5, 9, 21]



Investigation revolves around the transmission of eight-wavelength channels over turbulent HFFSO links using the WDM technique, with a proposed feeder fiber path length of 20 km for the system model [8, 15, 21] (<http://eprints.nottingham.ac.uk/13304/1/AladelobaAbisayoThesis.pdf>). Optical amplifiers (OAs) are deployed to enhance the device model post the receiver collection lens (RCL) to reduce inter-channel crosstalk in the system. The setup involves M-ary DPPM transmissions over OA and OBPF, converting OS to electrical signals at the receiver’s end, comprising elements such as a photodetector (PD), an electric amplifier, a filter, and decision circuitry alongside AO for modulation. The proposed system integrates hybrid pulse modulation/M-ary DPPM-M-PAPM for DWDM-FSO and hybrid optical fiber operation in turbulent atmospheric channels, transmitting information as a sequence of DPPM-M-PAPM pulses [21]. Specifically, the modulated signal from the M-ary DPPM-M-PAPM configuration is connected to OA and OBPF to produce M-ary DPPM-M-PAPM output, as shown in Fig. 1b [5, 9, 21]. For calculations, it is assumed that the loss of the signal multiplexer (mux) / demultiplexer (demux) does not exceed 3.5 dB [8, 15].

M-ary hybrid DPPM-M-PAPM modulation

Within this section, the MGF-based random variable (RV) characterizing the current $Y_{sig}(\Delta t)$ is explored, where $sig \in \{0, 1\}$ corresponds to whether pulses are transmitted or not for the signal pulses. Here, Δt represents the duration of the crosstalk pulse, which can be expressed as [5, 9, 19, 21–24]:

$$M_{Y_{sig}(\Delta t)}(s) = \left\{ \frac{R'G(e^{sq/t_s} - 1) \int_{t_s} sig P_{tr}(t) dt}{1 - R'N_o(e^{sq/t_s} - 1)} \right\} \frac{\exp\left\{ \frac{R'G(e^{sq/t_s} - 1) \int_{\Delta t} P_{XT}(t) dt}{1 - R'N_{o-XT}(e^{sq/t_s})} \right\}}{[1 - R'N_o(e^{sq/t_s} - 1)]} \quad (1)$$

where $\Delta t = t_s$ when aligning with the signal (OS) slots, otherwise t_1 or t_2 , and $\Delta t = 0$ signifies no crosstalk in the slot. Additionally, the strengths of the DPPM-PAPM pulse and ICC pulse are denoted as P_{tr} and P_{tr} respectively for the hybrid modulation techniques over the FSO link. The term $Rt = \eta/h\nu_i$, η is the PD quantum efficiency, ν_i, ν are the optical frequencies of ICC wavelengths and signal respectively, h represents Planck’s constant, and q is the electron charge [5, 8–10, 21, 25–30]. $N_o = 0.5(NF \times G - 1)h\nu$ is the OA power spectral density (PSD) at the single polarization ASE noise (ASEN). NF and G are the noise figure and OA gain G respectively, $L = B_o m_t t_s$ represents the system modes for the spatial and temporal approach [2, 8, 9, 31–38], B_o stands for the optical noise bandwidth for the demux channel and m_t denotes the quantity of ASE states. N_{o-XT} characterizes the PSD-ASEN at the PD and the signal-to-crosstalk ratio $C_{XT} = P_{tr}/P_{XT}$. The total MGF for Gaussian zero-mean,

including the thermal noise variance (TNV) is calculated as [5, 9, 21, 31–38]

$$M_{Y_{sig}(\Delta t)}(s) = M_{Y_{sig}(\Delta t)}(s) \exp\left(\frac{s^2 \sigma_{th-DPPM-PAPM}^2}{2} \right) \quad (2)$$

where $\sigma_{th-M-aryDPPM}^2$ is the TNV for M-ary DPPM-PAPM. The averages and standard deviations are provided as [5, 9]

$$\mu_{Y_{sig}(\Delta t)}(s) = \frac{LR'qN_o}{t_s} + R'Gq \left(sig P_{tr} \frac{P_{XT} \Delta t}{t_s} \right) \quad (3)$$

$$\sigma_{X_{sig}(\Delta t)}^2 = \sigma_{th-DPPM-PAPM}^2 + \left(\frac{LR'q^2 N_o (1 + R'N_o)}{t_s^2} \right) + R'Gq^2 \left[(1 + 2R'N_o) \frac{sig P_{tr}}{t_s} \right] + R'Gq^2 \left[(2R'N_{oXT}) \frac{P_{XT} \Delta t}{t_s^2} \right] \quad (4)$$

The symbol error probability (SER) is received in the exist of ICC $P_{ws(I_i-r_i)}$

$$P_{ws(I_i-r_i)} \geq \prod_{j \neq sigslot}^n P(X_1(\Delta t) > X_j) \quad (5)$$

where X_j denotes the non-signal slot $X_o(\Delta t_j)$ and Δt_j is the j^{th} (empty) slot overlap with the ICC. Using the GA, the expression $P\{X_o(\Delta t_j) > X_1(\Delta t)\}$ is explained from [1, 2, 5, 9, 10, 21, 25]

$$P\{X_o(\Delta t_j) > X_1(\Delta t)\} = 0.5 \operatorname{erfc} \left(\frac{\mu_{X_1(\Delta t)} - \mu_{X_o(\Delta t_j)}}{\sqrt{2(\sigma_{X_1}^2(\Delta t) + \sigma_{X_o}^2(\Delta t_j))}} \right) \quad (6)$$

In the proposed CB, we have fixed threshold T_{th} and the general form for RV (X) variable and a is $P(X > T_{th}) \leq E\{\exp [s (X - T_{th})]\}$, $s > 0$

$$P\{X_o(\Delta t_j) > X_1(\Delta t)\} \leq M_{X_1(\Delta t)}(-s)M_{X_o(\Delta t)}(s) \quad (s > 0) \quad (7)$$

For the MCB [2, 5] of two RVs for $X_o(\Delta t_j)$ and $X_1(\Delta t)$, $P(X > T_{th}) \leq M_X(s)e^{-sT_{th}}/s\sigma_{th}\sqrt{\pi}$ [5, 9, 10]. Modifying this inequality for the difference of RVs s for $X_o(\Delta t_j)$ and $X_1(\Delta t)$ which both have the same TNV then [21]

$$P\{X_o(\Delta t_j) > X_1(\Delta t)\} \leq \frac{M_{X_1(\Delta t)}(-s)M_{X_o(\Delta t)}(s)}{2s\sigma_{th}\sqrt{\pi}} \quad (8)$$

The SER for MDPPM-MPAPM frames in the exist of ICC is written as [1, 9, 10, 21]

$$P_{we(t_s-r_s)} \leq 1 - [1 - P\{X_o(0) > X_1(\Delta t)\}]^{n-1} [1 - P\{X_o(t_s) > X_1(\Delta t)\}]^{1-s-r_s} \quad (9)$$

where and I_s, r_s are the numbers of ICC system of duration t_s occurring in the frame and signal pulse respectively [38],

$$P_{we(I_1, I_2 - r_1, r_2)} \leq 1 - [1 - P\{X_o(0) > X_1(\Delta t)\}]^{n-1-\bar{X}} [1 - P\{X_o(t_1) > X_1(\Delta t)\}]^{1-r_1} [1 - P\{X_o(t_2) > X_1(\Delta t)\}]^{1-r_2} \tag{10}$$

where I_1, I_2 , and r_1, r_2 represent the ICC duration t_1, t_2 $\bar{X} = I_s - r_s$. The bit error rate (BER) when there is no ICC is described as [21]

$$BER_{I_s}(n_1) = P_{f(I_s)}(n_1) = \frac{n}{2(n-1)} \times (P_{f(I_s)}(1)P_{we(I_s-1)} + P_{s(I_s)}(0)P_{we(I_s-0)}) \tag{11}$$

The BER is computed as:

$$BER = \frac{1}{n} \sum_{n_1=1}^n \sum_{I_s=0}^2 BER_{I_s}(n_1) \tag{12}$$

For the BER calculation, it is expressed as:

$$BER(n_1) = P_{f(0,0)}(n_1) \frac{n}{2(n-1)} P_{we(0,0-0,0)} \tag{13}$$

Regarding the calculated BER, it is determined as [1, 2, 5–10, 21, 25, 31–38]:

$$BER_{I_1, I_2}(n_1) = \frac{1}{n} \sum_{I_1=I_2}^{I_s} P_{f(I_1, I_2)}(n_1) \frac{n}{2(n-1)} \left\{ \left[\frac{P_{s(I_1, I_2)}(1, 0)P_{we(I_1, I_2, 1, 0)}}{P_{s(I_1, I_2)}(0, 1)P_{we(I_1, I_2, 0, 1)}} \right] + P_{s(I_1, I_2)}(0, 0)P_{we(I_1, I_2, 0, 0)} \right\} \tag{14}$$

In the presence of ICC, the overall BER of the M-ary-DPPM-M-PAPM is derived from Eqs. (13) and (14) [1, 2, 21, 25]:

$$BER_{M\text{-ary-DPPM-M-PAPM}} = \frac{1}{n} \sum_{n_1=1}^n \left\{ \begin{aligned} &BER(n_1) + BER_{0,1}(n_1) + BER_{1,0}(n_1) \\ &+ \sum_{I_1=1}^2 [BER_{I_1,1}(n_1) + BER_{I_1,2}(n_1)] \end{aligned} \right\} \tag{15}$$

Adverse atmospheric channel

The scintillation effects are influenced by differences in the air, variations in the refractive index structure (RIS) C_n^2 , and the Earth’s surface temperature [5, 8, 21]. These research findings focus on the probability density function (pdf) of the Gamma-Gamma (GG) model [5, 8–10, 21, 25–30].

$$P_{GG}(h_Z) = \frac{2(\alpha\beta)^{(\alpha+\beta)/2}}{\Gamma(\alpha)\Gamma(\beta)} h_Z^{(\alpha+\beta)/2-1} K_{\alpha-\beta}(2\sqrt{\alpha\beta}); h_Z > 0, \tag{16}$$

where h_Z represents the total attenuations due to the signal (h_{sig}) and interfering (h_{int}) and pointing errors. α and β refer

to the scattering mechanisms of the influence of large and small-eddies, respectively, $\Gamma(\bullet)$ is the gamma function, and $K_n(\bullet)$ is the modified second kind Bessel function [8–10, 21].

$$\alpha = \left\{ \exp \left[\frac{0.49\sigma_R^2}{(1 + 0.65d^2 + 1.11\sigma_R^{12/5})^{7/6}} \right] - 1 \right\}^{-1} \tag{17}$$

$$\beta = \left\{ \exp \left[\frac{0.51\sigma_R^2 (1 + 0.69\sigma_R^{12/5})^{-5/6}}{1 + 0.9d^2 + 0.62d^2\sigma_R^{12/5}} \right] - 1 \right\}^{-1} \tag{18}$$

$$d = \sqrt{kD_{RX}^2/4l_{fso}} \tag{19}$$

Here, d symbolizes the normalized RCLs [8–10, 21, 26, 29] and D_{RX} is the RCL diameter C_n^2 is the RIS constant, l_{fso} is the free-space distance, $k = 2\pi/\lambda$ is the wave-number, and λ is the wavelength [21, 25, 26, 30–36]. The Rytov variance (RVAR) σ_R^2 signifies the various AT regimes within the GG pdf. If $\sigma_R^2 > 1$, the ST model is utilized; if $\sigma_R^2 \approx 1$, the MT model is applied, and $\sigma_R^2 < 1$, the WT model is used [8–10, 25]. Additionally, in instances of saturated turbulence where $\sigma_R^2 \rightarrow \infty$ as described in [8–10, 21, 36–42].

$$\sigma_R^2 = 1.23C_n^2 k^{7/6} l_{fso}^{11/6} \tag{20}$$

When introducing the Gaussian receiver TNV, the overall MGF is derived [5–10, 17, 21, 31–38].

$$M_{Z_j}(s/I) = M_{th}(s)M_{Y_j}(s/I), \tag{21}$$

The thermal noise MGF, given by $M_{th}(s)M_{Y_j} = \exp(\sigma_m^2 s^2/2)$, is calculated where σ_m^2 represents the TNV at the decision circuit [17, 30, 36] (<http://eprints.nottingham.ac.uk/13304/1/AladelobaAbisayoThesis.pdf>). The BER for a given irradiance I is expressed as [5–10, 17, 21, 31–38].

$$BER(I) = \frac{1}{2} [P(1|0, I) + P(0|1, I)], \tag{22}$$

The probabilities $P(1|0, I)$ describe the likelihood of receiving a specific signal given the transmission and irradiance [5–10, 17, 21, 31–38].

$$P(1|0, I) = P(i_o(I) > i_D(I)) \leq \exp(-s_0 i_D(I)) M_{Z_0}(s_0, I), \quad s_0 > 0 \tag{23}$$

$$P(0|1, I) = P(i_I(I) > i_D(I)) \leq \exp(-s_1 i_D(I)) M_{Z_1}(s_1, I), \quad s_0 > 0 \tag{24}$$

These probabilities are defined based on the decision threshold $i_D(I)$. The CB defines the upper boundary for the BER as

$$\text{BER}_{\text{CB}}(I) = \frac{1}{2} [\exp(-(-s_{iD}(I)) M_{Z_0}(s, I) + \exp(s_{iD}(I)) M_{Z_1}(-s, I))] \tag{25}$$

$s = s_0 = s_1 > 0$

where $M_{Z_0}(s, I)$ and $M_{Z_1}(s, I)$ are given by Eq. (21). The setting of s is a very small accuracy power [5–10]. By replacing the optical link length z with l_{fso} , the beam-width of a Gaussian beam w_z due to the AT effects increase with the link length $z = l_{fso}$, and it is given as [5–10, 17, 21, 31–38]

$$w_z = w_0 \left(\sqrt{1 + (z/z_L)^2} \right) \times \left(\sqrt{1 + 1.33\sigma_R^2 \left(2z/kw_0 \sqrt{1 + (z/z_L)^2} \right)^{5/6}} \right) \tag{26}$$

where w_0 is the minimum value of w_z at a point ($z=0$) and $z_L = \pi w_0^2/2$ is called the Rayleigh range. The combined pdf due to PE and geometric spread (GS) are represented as [5–10, 17, 31–38]

$$p_{PE}(h_p) = \frac{\gamma^2}{A_0^2} h_p^{\gamma^2-1}; \quad 0 \leq h_p \leq A_0, \tag{27}$$

where h_p signifies attenuation attributable to GS and PE, $\gamma = w_{zeq}/2\sigma_{PE}$, represents the impact of jitter-induced PE at the receiver characterized by σ_{PE} , $w_{zeq}^2 = w_z^2 \sqrt{\pi} \text{erf}(v)/2v \exp(-v^2)$ denoting the equivalent beam-width square [17, 21, 31–38], $A_0 = [\text{erf}(v)]^2$ denotes the portion of power collected with zero radial displacement [30, 32, 36], and $v = (\sqrt{\pi} r_{RX}) / (\sqrt{2} w_z)$ [31–38]. The combined pdf due to AT, PE, and GS is given as [5–10, 17, 31–38]

$$p(h_{tot}) = \int p_{PE}(h_{tot}|h_a) p_{GG}(h_a) dh_a, \tag{28}$$

where $h_{tot} = h_a h_p$ and p_{PE} is the probability distribution for PE conditioned on h_a , such that [5–10, 17, 31–38]

$$\int p_{PE}(h_{tot}/h_a) = \frac{1}{h_a} p_{PE}\left(\frac{h_{tot}}{h_a}\right) = \frac{\gamma^2}{A_0^2} \left(\frac{h_{tot}}{h_a}\right)^{\gamma^2-1}; \quad 0 \leq h_{tot} \leq A_0. \tag{29}$$

On substituting Eqs. (16) and (29) into Eq. (30), the combined pdf can be re-written as [5–10, 17, 21, 31–38]

$$P_{GG}(h_{tot}) = \frac{2\gamma^2(\alpha\beta)^{(\alpha+\beta/2)}}{A_0^2 \Gamma(\alpha)\Gamma(\beta)} h_{tot}^{\gamma^2-1} \times \int_{h_{tot}/A_0}^{\infty} h_a^{(\frac{\alpha+\beta}{2}-1-\gamma^2)} K_{\alpha-\beta}(2\sqrt{\alpha\beta}h_a) dh_a; \tag{30}$$

The DPPM BER is given by [5–10, 17, 31–38],

$$\text{BER}(h_{\text{turb}}, P) = \frac{n P_{\text{we}}(h_{\text{turb}}, P)}{2(n-1)}, \tag{31}$$

where the symbol error probability $P_{\text{we}}(h_{\text{turb}}, P) = 1 - P_{\text{we}}(h_{\text{turb}}, P)$ is bounded by $\{X_{tr} > X_1\}, \dots, \{X_{tr} > X_j\}, \dots, \{X_{tr} > X_n\}$ [5–10, 17, 21, 31–38]

$$P_{\text{ws}}(h_{\text{turb}}, P) \geq \prod_{\substack{j=1 \\ j \neq \text{tr}}}^n P(X_{tr} > X_j | h_{\text{turb}}, P) = (P(X_{tr} > X_f | h_{\text{turb}}, P))^{n-1}, \tag{32}$$

Then $P_{\text{we}}(h_{\text{turb}}, P)$ can be expressed as [5–10, 17, 31–38]

$$P_{\text{we}}(h_{\text{turb}}, P) \leq 1 - (P(X_f > X_{tr} | h_{\text{turb}}, P))^{n-1}, \tag{33}$$

Assuming that the random variables X_{tr} and X_f are Gaussian [31–38], the GA expression formula for $P_{\text{we,GA}}(h_{\text{turb}}, P)$ is derived by employing Eq. (33) [5–10, 17, 21, 31–38]

$$P_{\text{we,GA}}(h_{\text{turb}}, P) \leq 1 - \left(1 - 0.5 \text{erfc} \left(\frac{\mu_{X_{tr}}(h_{\text{turb}}, P) - \mu_{X_f}}{\sqrt{2(\sigma_{X_{tr}}^2(h_{\text{turb}}, P) + \sigma_{X_f}^2)}} \right) \right)^{n-1}, \tag{34}$$

$$P(X_f > X_{tr} | h_{\text{turb}}, P) \leq M_{X_f}(s | h_{\text{turb}}, P) M_{X_{tr}}(-s | h_{\text{turb}}, P) \quad (s > 0), \tag{35}$$

$$P_{\text{we,CB}}(h_{\text{turb}}, P) \leq 1 - (1 - M_{X_{tr}}(-s_{\text{opt}} | h_{\text{turb}}, P) M_{X_f}(s_{\text{opt}} | h_{\text{turb}}, P))^{n-1}, \tag{36}$$

The general formula for the MCB is expressed as $P(X > \varphi) \leq \exp(-s\varphi) M_X(s) / s\sigma_{th} \sqrt{2\pi}$, where φ is a constant and X involves the variance σ_{th}^2 [5–10, 17, 31–38].

$$P(X_f > X_{tr} | h_{\text{turb}}, P) \leq \frac{M_{X_f}(s | h_{\text{turb}}, P) M_{X_{tr}}(-s | h_{\text{turb}}, P)}{s\sigma'_{th} \sqrt{2\pi}}, \tag{37}$$

This MCB expression (Eq. 37) is then combined with Eq. (33) to calculate $P_{\text{we,MCB}}(h_{\text{turb}}, P)$ [5–10, 17, 31–38]

$$P_{\text{we,MCB}}(h_{\text{turb}}, P) \leq 1 - \left(1 - \left(\frac{M_{X_{tr}}(-s_{\text{opt}} | h_{\text{turb}}, P) M_{X_f}(s_{\text{opt}} | h_{\text{turb}}, P)}{2s\sigma'_{th} \sqrt{2\pi}} \right) \right)^{n-1} \tag{38}$$

The overall DPPM BER is provided by [5–10, 17, 31–38]

$$\text{BER}_{Z,GG}(P) = \int_0^{\infty} \text{BER}_Z(h_{\text{turb}}, P) p_{GG}(h_{\text{turb}}) dh_{\text{turb}} \tag{39}$$

where $\text{BER}_Z(h_{\text{turb}}, P)$ involves the BERs derived from Eq. (31) using the $P_{\text{we}}(h_{\text{turb}}, P)$ boundaries from Eqs. (34), (36) and (38) ($Z = \text{GA, CB, and MCB}$) [5–10, 17, 30–38].

Results and discussions

The outcomes and discussions are presented in Table 1, displaying the recommended system model parameters alongside values extracted from multiple references [2, 38] (<http://eprints.nottingham.ac.uk/13304/1/AladelobaAbisayoThesis.pdf>) used in establishing the system architecture. The proposed design parameters are listed in Table 1, accompanied by an examination of how turbulence impacts system performance, particularly concerning OOK-M ary-DPPM modulation in relation to M-ary DPPM-PAPM and other atmospheric conditions. Figure 2 illustrates the significant impact of atmospheric turbulence (AT) when the channel BER is high, with both MCB and CB exhibiting similar trends, albeit with an increase in AT strength as referenced [9, 10, 39–42]. Graphs depicting CB and MCB show variations from the general pattern observed in Ref. [38], where $G = 27$ dB, contrasting with the current work displaying $G = 30$ dB concurrently with the ICC showcased in Fig. 3. Specifically, for $M = 2$ and $G = 8$ dB, the current study presents outputs related to MCB, CB, and GA. At low G levels, MCB closely aligns with GA, as depicted in Fig. 3a, while at higher gains, it approximates CB more closely, with the decrease in ASEN impacting the TNV results. Additionally, GA outperforms CB and MCB when the ICC is absent at high G levels, extending the coding level (CL) and bandwidth of the DPPM-PAPM receiver concerning the noise equivalent. Furthermore, the GA margin proves more extensive than the MCB of PAPM-M-DPPM. The corresponding output of MCB, CB, and GA for $G = 8$ dB with $M = 2$ is shown in Fig. 3b, aligning with the validated findings in Ref. [38]. Notably, MCB mirrors GA at lower G values but diverges towards CB as ASEN decreases, thereby influencing TNV outcomes [39–42].

In the scenario of BER targets at levels of 10^{-12} , the methods of MCB, CB, and GA were employed for ST and WT using MCB, CB, and GA. This involved configuring the receiver sensitivity (RS) for $G = 30.6$ dB and

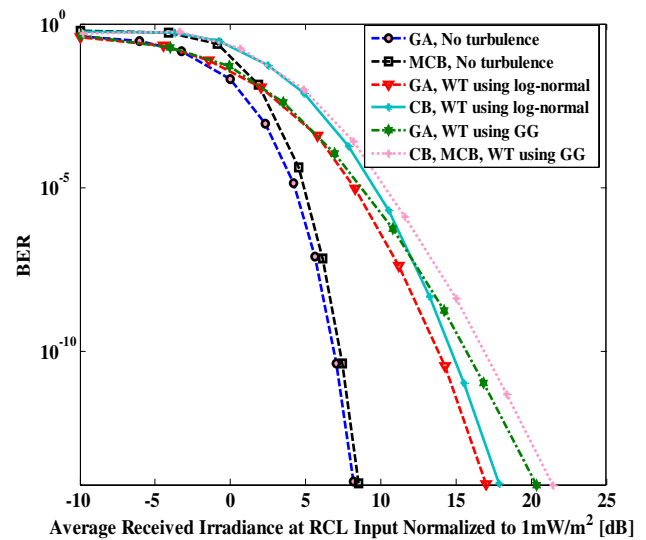


Fig. 2 The BER plotted against average irradiance [dB] for scenarios no turbulence (NT) and with atmospheric turbulence using the GG model and log-normal distribution

$l_{fso} = 1500$ m [2, 9, 36] as indicated in Fig. 4a and b. Results depicted RS values of -51.49 dBm (CB), -51.59 dBm (MCB), and -50.53 dBm (GA), showcasing enhancements and optimizations achieved in [2, 9, 36]. Additionally, for $G = 30$ dB and (l_{fso}) = 2500 m at the same BER target of 10^{-12} , RS values of -51.49 dBm (CB), -51.56 dBm (MCB), and -50.25 dBm (GA) were presented [Proposed work]. Figure 5 displays the performance of BER against Optical Signal-to-Noise Ratio (OSNR) in decibels for the DWDM-PON/HFFSO link employing a combination of OOK/M-ary DPPM and M-PPM under the configuration with CL $M = 5$, $l_{fso} = 4000$ m, and $D_{RX} = 25$ mm for ST. The hybrid OOK/M-ary DPPM-PAPM method demonstrates enhancements of approximately 4 dB, 6 dB, and 8 dB in OSNR compared to the respective 3-DPPM, 4-DPPM, and 5-DPPM schemes of ST within the

Table 1 System parameters were employed in the computational analysis presented in references [2, 38] (<http://eprints.nottingham.ac.uk/13304/1/AladelobaAbisayoThesis.pdf>) and [Proposed Work]

Parameters	Description	Ref. [2] (http://eprints.nottingham.ac.uk/13304/1/AladelobaAbisayoThesis.pdf)	Ref. [38]	[Proposed work]
R_b	Data rate	2.5 Gbps	2.5 Gbps	2.5 Gbps
B_o	Demux OBPF bandwidth	80 GHz	76 GHz	80 GHz
λ_{sig}	Wavelength	1550 nm	1550 nm	1550 nm
η	Quantum efficiency	0.75	0.9	1
G	OA gain	30.6 dB or 8.8 dB	27 dB or 8 dB	30 dB or 8 dB
NF	OA noise figure	4.77 dB [2]	4.77 dB [2]	4.77 dB [2]
l_{fso}	Maximum FSO link length	1000 m and 1500 m	1000 m and 1500 m	1500 m—4000 m
m_t	ASE noise polarization states	2	2	2

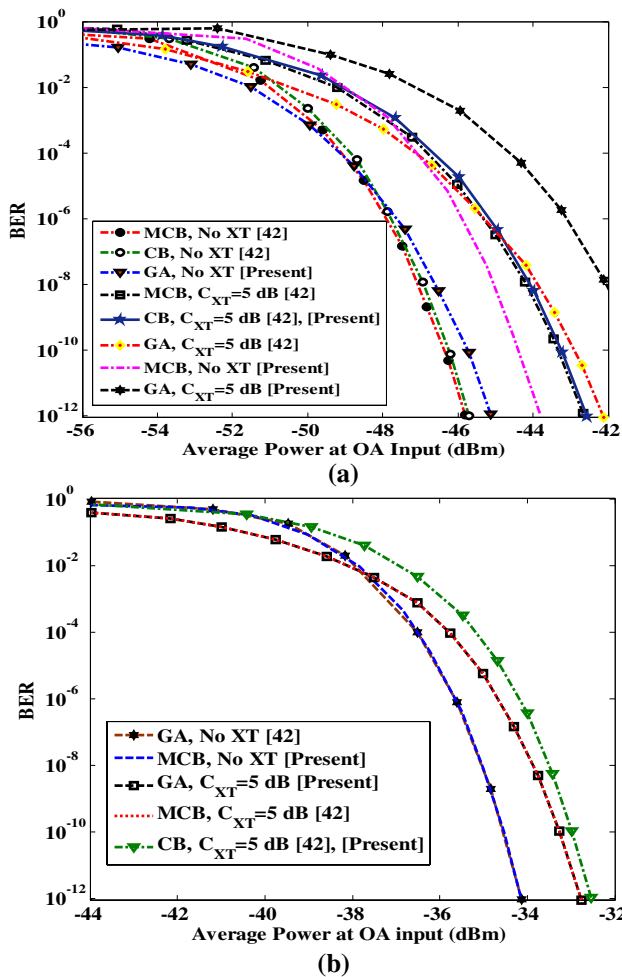


Fig. 3 The BER is shown against the average optical power (AOP) in (dBm) for two cases: (a) $G=27$ dB [38] at 1500 m and $G=30$ dB [present study] at 4000 m, and (b) $G=8$ dB demonstrated in [38] at 1500 m and in the current study at 4000 m

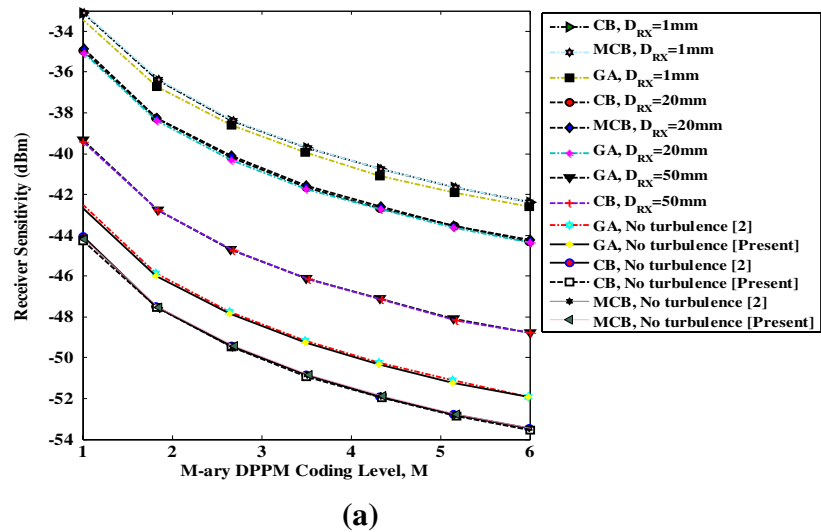
DWDM-HFFSO fiber network at a specified BER level of 10^{-12} . It was noted that ST without the hybrid OOK/M-ary modulation approach required higher power levels due to the influence of AT effects, ICC, and ASE noise to achieve a comparable BER performance when contrasted with ST using the hybrid OOK/M-ary DPPM strategy, as depicted in Fig. 5. This indicates that the hybrid modulation scheme OOK/M-ary DPPM-PAPM, based on WDM-HFFSO communication, is favored for ensuring enhanced efficiency and superior performance in our design. The target BER of 10^{-10} is achieved for values of ($m \geq 100$), while the BER significantly deteriorates at higher ICC and lower CL values for ($m \leq 100$), as illustrated in Fig. 6. For a target BER of 10^{-9} , the analysis of DPPM PP for ICC ($M=2$) is compared to OOK, as shown in Fig. 7. The M-DPPM-M-PAPM combination demonstrates lower PP values than OOK. The enhancement in PP due to M-DPPM-M-PAPM

is magnified as the CL number advances from ($M=1$) to (2) and with the influence of ICC sources [5, 8, 9, 42–52]. The proposed M-ary DPPM-M-PAPM technique boosts receiver sensitivity in WDM-M-HFFSO systems compared to OOK-NRZ, resulting in improved reliability and a reduced PP ranging from 0.2 to 3.0 dB for WT. Failing to adapt to achieve a BER of 10^{-12} led to a 4 dB decrease in OSNR due to modulation techniques, as demonstrated in Fig. 8.

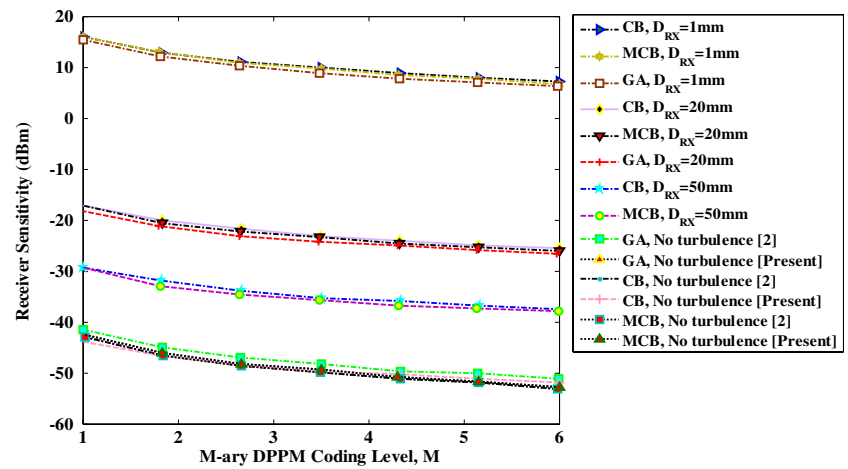
Compared to the hybrid OOK/M-ary DPPM, the M-n-PAPM requires an additional 0.3 dB of power. The study illustrates that enhancing the proposed hybrid OOK/M-DPPM and M-n-PAPM models for WDM-FSO systems is feasible [50–56]. Table 2 delineates the suggested modulation strategies of MPPM, M-ary-PAPM, and the combined M-ary PAPM-MPPM with the hybrid k-level n-pulse where k^n (with $k \in \{1, 2, \dots\}$) [2, 8, 9, 21, 38, 46] (<http://eprints.nottingham.ac.uk/13304/1/AladelobaAbisayoThesis.pdf>). Figure 9 depicts BER vs. the average RCL power input (dBm), $D_{RX} = 25$ mm for M-ary DPPM and OOK for NT and (a) WT (b) MT and (c) ST for M-ary DPPM and $G=30$ dB, $M=5$. Achieving a BER target of 10^{-12} , DPPM enhances sensitivity by approximately 10–11 dB compared to OOK-NRZ, as evidenced in Fig. 9a [2, 9, 10, 21, 38–43, 52–58] (<http://eprints.nottingham.ac.uk/13304/1/AladelobaAbisayoThesis.pdf>). When experiencing a deficit in the AT, DPPM's overall sensitivity declines to about 10 dB (WT), 8 dB (MT), and 8 dB, respectively (ST). The OOK-NRZ-based FSO system demonstrates an improvement of around 7–9 dB over the DPPM scheme, as portrayed in Fig. 9b [2, 9, 21]. With an AT deficiency, DPPM's sensitivity is reduced to about 7 dB (WT), 8 dB (MT), and 8 dB (ST) [2, 9, 10, 21, 38–43] (<http://eprints.nottingham.ac.uk/13304/1/AladelobaAbisayoThesis.pdf>), respectively, as shown in Fig. 9c.

The hybrid M-ary PAPM-DPPM modulation offers a significant improvement of approximately 10–11 dB in OOK-NRZ sensitivity within the WDM-FSO optical fiber network system when turbulent conditions are not present. This sensitivity enhancement is demonstrated in Fig. 10 [44–54]. However, in the presence of turbulence and ASE noise, the decrease in sensitivity of PAPM-DPPM compared to OOK-NRZ is noted as 10 dB (WT), 8 dB (MT), and 8 dB (ST) [current]. Ensuring and consistently maintaining the accuracy of simulation models and algorithms is crucial by verifying simulation results through cross-referencing with experimental findings from previous studies [2, 5, 8, 9, 15, 21, 38, 46, 51–58]. Furthermore, our research successfully compares previous work and evaluates them against new model results [59–62]. Tables 1, 3, and 4 provide a detailed description of the specific system parameters used in previous studies [2, 5, 8, 9, 15, 21, 38, 46], and the [proposed work]. The simulation results indicate that the WDM/

Fig. 4 The receiver sensitivity (RS) in (dBm) versus the M-ary DPPM coding level for NT under both (a) WT and (b) ST conditions as depicted in [2] and the current study



(a)



(b)

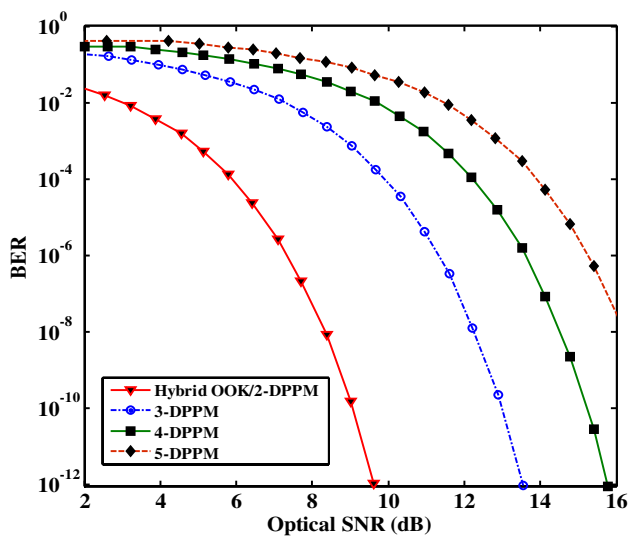


Fig. 5 The BER plotted against Optical Signal-to-Noise Ratio (OSNR) in (dB) using $D_{RX} = 25$ mm, $M = 5$, $I_{fso} = 4000$ m for ST

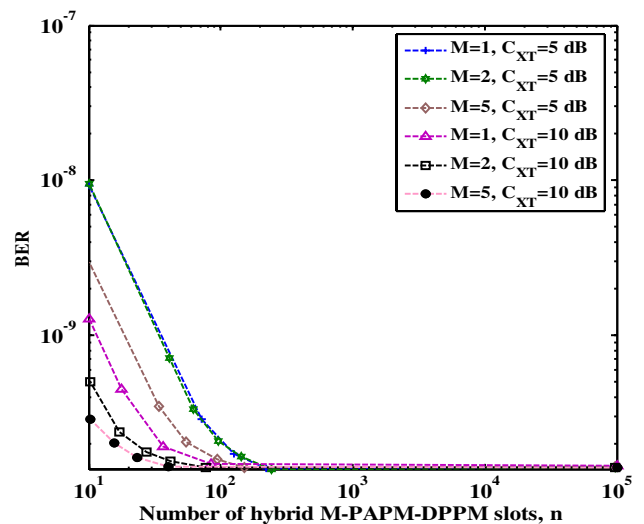


Fig. 6 The graph shows the relationship between bit error rate (BER) and slot numbers (n) for the hybrid M-DPPM-M-PAPM using MCB with a gain of 30 dB

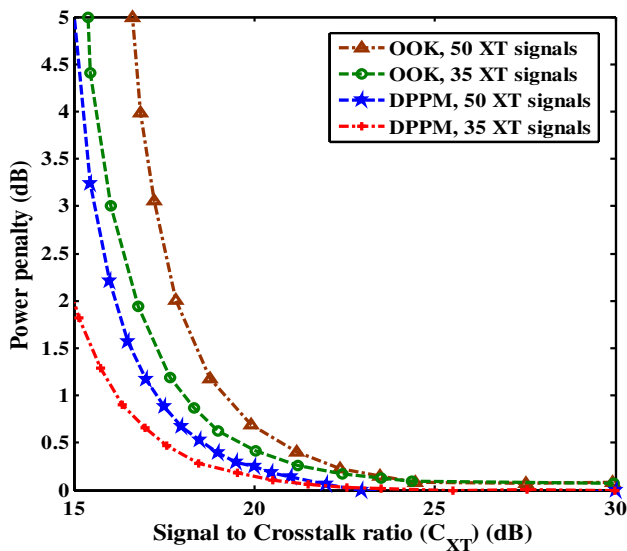


Fig. 7 The power penalty versus crosstalk (CXT) (dB) for OOK compared to DPPM-M-PAPM at $M=2$ and OOK/M-DPPM-M-PAPM at a BER of 10^{-9} for crosstalk signals at 35 and 50

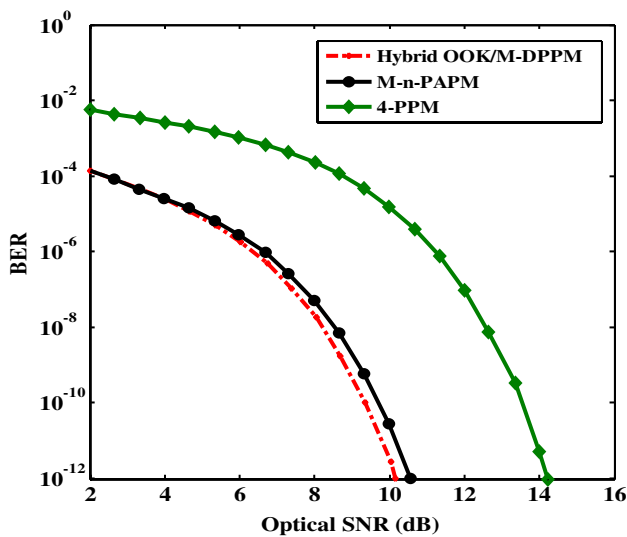


Fig. 8 The BER vs. OSNR (dB) to for the hybrid OOK/M-ary DPPM and M-n-PAPM modulation scheme

Table 2 The suggested modulation schemes for the DWDM-FSO optical fiber communication network system is based on the M-ary DPPM-M-PAPM design [2, 5, 8, 9, 21, 38, 46] (<http://eprints.nottingham.ac.uk/13304/1/AladeIobaAbisayoThesis.pdf>)

Modulation Scheme	Bits per Symbol	Bandwidth Requirement	Spectral Efficiency
MPPM	$\left\lfloor \log_2 \left(\frac{M}{n} \right) \right\rfloor$	$\frac{MR_b}{\left\lfloor \log_2 \left(\frac{M}{n} \right) \right\rfloor}$	$\frac{\left\lfloor \log_2 \left(\frac{M}{n} \right) \right\rfloor}{M}$
M-ary-PAPM	$\left\lfloor \log_2 k^n \left(\frac{M}{n} \right) \right\rfloor$	$\frac{MR_b}{\left\lfloor \log_2 \sum_{i=1}^n \left(\frac{M}{n} \right) \right\rfloor}$	$\frac{\left\lfloor \log_2 k^n \left(\frac{M}{n} \right) \right\rfloor}{M}$
Hybrid M-ary PAPM-MDPPM	$\left\lfloor \log_2 k^n \sum_{i=1}^n \left(\frac{M}{i} \right) \right\rfloor$	$\frac{MR_b}{\left\lfloor \log_2 k^n \sum_{i=1}^n \left(\frac{M}{i} \right) \right\rfloor}$	$\frac{\left\lfloor \log_2 k^n \sum_{i=1}^n \left(\frac{M}{i} \right) \right\rfloor}{M}$

PAPM-DPPM system’s bit error rate outperforms that of OOK-NRZ by approximately 10 dB to 11 dB at a level of 10^{-12} . Table 3 provides a comprehensive comparison of the operational efficiency of the innovative hybrid M-ary-PAPM M-DPPM-based DWDM FSO optical fiber network link with references to existing literature [2, 5, 8, 9, 15, 38]. The numerical data underscores the effectiveness of the M-ary-PAPM M-DPPM-based DWDM FSO network, uniquely crafted to integrate a DWDM-PON optical fiber infrastructure. The numerical analysis clearly demonstrates that the proposed link’s performance improves with enhanced receiver sensitivity, capacity, and operational efficiency, particularly in the presence of atmospheric turbulence. A comparative analysis of the performance of the M-ary DPPM-M-PAPM-based DWDM-FSO optical fiber communication system against current literature underscores the superior performance of the proposed link in terms of maximum range, efficiency, and channel capacity. The impact of ASE noise, AT channels, and ICC on DWDM-FSO optical fiber communication systems is addressed. Table 4 presents performance comparisons, showcasing the superiority of the proposed M-ary DPPM-M-PAPM-based DWDM-FSO optical fiber link with reference to [46]. The innovative hybrid M-ary-PAPM M-DPPM configuration provides a substantial enhancement of 4–8 dB at a bit error rate of 10^{-12} (OSNR) [proposed work], whereas Ref. [46] indicates an improvement of 1 and 2 dB at a Bit Error Rate of 10^{-6} .

Figure 11 shows the MCB BER as a function of average transmitted optical power (dBm) for $\sigma_{PE}/I_{RX} = 0.1, 3 \& 5$, $M=5$, $G=30$ dB with $D_{RX} = 50$ mm. Specifically, in the ST scenario illustrated in Fig. 2, a significant improvement is seen in the required power by approximately 14 dB (for the ST with GS) case and 22 dB for ($\sigma_{PE}/I_{RX} = 3$) and 2 dB (for $\sigma_{PE}/I_{RX} = 3$) (ST, PE, and GS case) at target BER of 10^{-9} . Furthermore, at a target BER of 10^{-12} , by using a coding level of 5 for NT with GS and $D_{RX} = 50$ mm, DPPM manifests about a 9 dB sensitivity enhancement over the OOK-NRZ FSO system, as shown in Fig. 11. Moreover, in Fig. 12, an enhancement in the required optical power of roughly 10 dB with GS of the DPPM case over the OOK-NRZ for the NT scenario in the DWDM/FSO system can be observed. In the

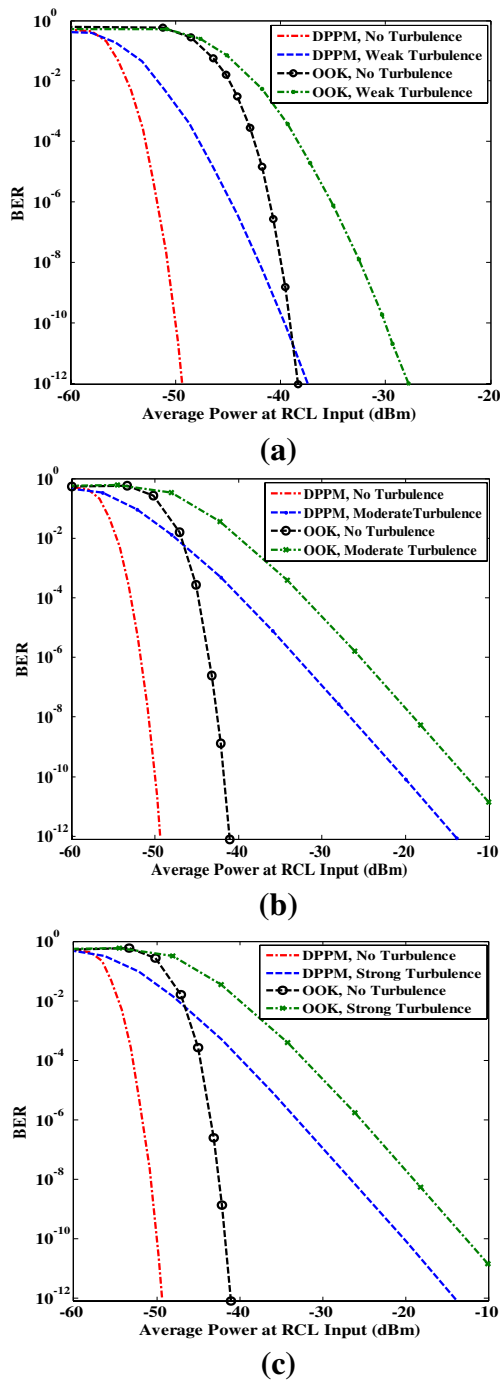


Fig. 9 The graph shows the relationship between BER and average optical power (AOP) at the RCL input in (dBm) for M-ary DPPM and OOK using $D_{RX} = 25$ mm, $G = 30$ dB, $M = 5$, and $l_{fso} = 4000$ m for NT with (a) WT, (b) MT, and (c) ST

ST case with GS at $\sigma_{PE}/\Gamma_{RX} = 6$, an improvement in the necessary optical power of around 10 dB of the DPPM over the OOK-NRZ system is noted. When aiming for a target BER using MCB, in the MT scenario with PE at $\sigma_{PE}/\Gamma_{RX} = 4$, the M-ary DPPM offers about 8.0–9.0 dB sensitivity

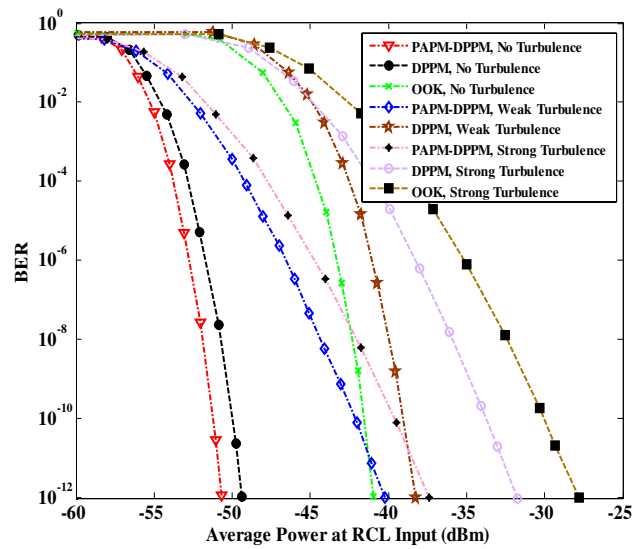


Fig. 10 The BER against AOP at the RCL input (dBm) for DPPM and OOK under conditions of no turbulence and WT

enhancement over the OOK-NRZ in the absence of turbulence [10, 25, 35–38]. Additionally, in Fig. 13, BER curves are presented for FSO at $l_{fso} = 2000$ m and $l_{fso} = 2400$ m, employing $G = 30$ dB, $D_{RX} = 4$ mm, and $M = 5$ for the NT scenario with WT, MT, and ST regimes, respectively. Notably, atmospheric turbulence effects become more pronounced for longer link lengths; for instance, at the target BER, the receiver sensitivity deteriorates by about 6 dB (WT), 13 dB (MT), and 9 dB (ST) as the FSO link length increases from 2000 to 2500 m [6, 10, 17, 25, 30, 32, 36, 38] (<http://eprints.nottingham.ac.uk/13304/1/AladelobaAbisayoThesis.pdf>). Figure 14a and b demonstrate the impact of increasing the receiver aperture diameter on the capacity within a ST scenario with and without PEs respectively. It is observed that the ASE (bits/s/Hz) reaches saturation levels when the aperture diameter exceeds 8 cm and 10 cm [63]. By utilizing aperture averaging (AA), a hybrid M-ary hybrid DPPM-M-PAPM scheme, and spatial diversity [64], we achieved an ASE (bits/s/Hz) performance of 53 bit/s/Hz and 38 bit/s/Hz without and with PEs, respectively. This was achieved at an aperture diameter of 10 cm and an ATOP of 13 dBm, as depicted in Fig. 14. The BER curves and Performance Analysis section discusses the BER curves for FSO links at different lengths and configurations. These include NT with WT, MT, and ST regimes. Furthermore, the impact of increasing the receiver aperture diameter on the capacity and ASE performance is analyzed in the ST scenario, both with and without PE effects. The numerical results provide insights into the performance and effectiveness of the M-ary hybrid DPPM-M-PAPM modulation scheme under various scenarios and conditions. Additionally, a sensitivity comparison between M-ary DPPM and OOK-NRZ in the absence of turbulence is discussed for the

Table 3 The performance of the proposed M-ary DPPM-M-PAPM based DWDM-FSO optical fiber link is compared with existing literature [2, 5, 8, 9, 15, 38]

	Ref. [2]	Ref. [5]	Ref. [8]	Ref. [9]	Ref. [15]	Ref. [38]	[Proposed work]
Technique used	DPPM-FSO link	WDM-FSO hybrid fiber-based DPPM	DPPM- based DWDM-FSO system	M-ary PPM- based WDM -FSO system	WDM-FSO network-based DPPM modulation	DPPM-based WDM-FSO communication system	hybrid M-ary-PAPM M-DPPM-based DWDM FSO optical fiber network
Data rate	2.5 Gbps	2.5 Gbps	2.5 Gbps	2.5 Gbps	2.5 Gbps	2.5 Gbps	2.5 Gbps
Net capacity	2.5 Gbit/s	5 Gbit/s	20 Gbit/s	20 Gbit/s	5 Gbit/s	5 Gbit/s	20 Gbit/s
Maximum link range reported	1500 m	2000 m	4000 m	2500 m	2000 m	2000 m	4000 m
Quantum efficiency	0.75	0.8	1	1	0.8	0.9	1
No. of channels	1	2	8	8	2	2	8
Target BER	10^{-12}	10^{-12}	10^{-12}	10^{-12}	10^{-12}	10^{-12}	10^{-12}

Table 4 Performance comparison of the M-ary DPPM-M-PAPM based DWDM-FSO optical fiber link with the reference [46]

	Ref. [46]	[Proposed work]
Technique for modulation scheme	hybrid M-PAPM technique for deep space optical communication link	hybrid M-ary M-DPPM-M-PAPM FSO based DWDM optical fiber communication network
OSNR improved	1 dB and 2 dB	4–8 dB
Desired BER	10^{-6}	10^{-12}
The number of optical pulses per frame for m	16	16

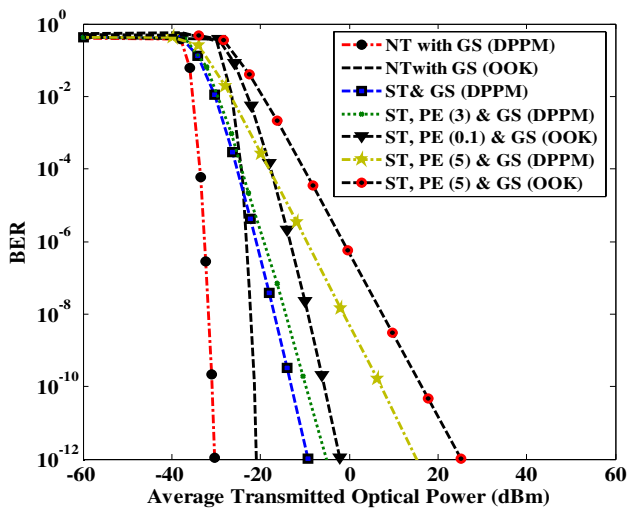


Fig. 11 MCB BER in relation to the average transmitted optical power (ATOP) (dBm) for $\sigma_{PE}/\Gamma_{RX} = 0.1, 3 \text{ \& } 5$, $D_{RX} = 50 \text{ mm}$, $G = 30 \text{ dB}$, and $M = 5$

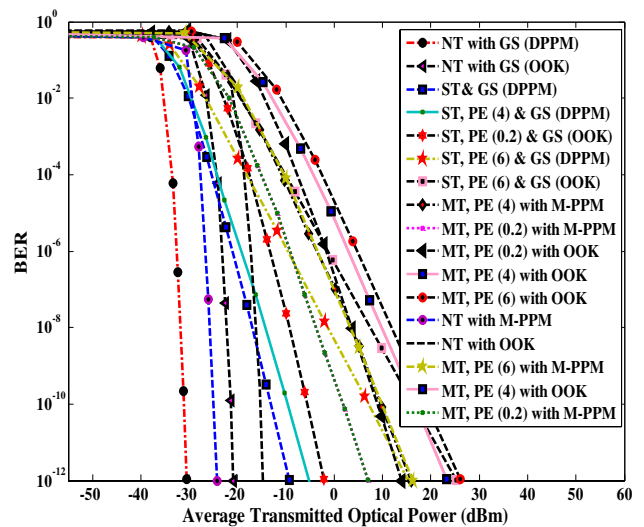
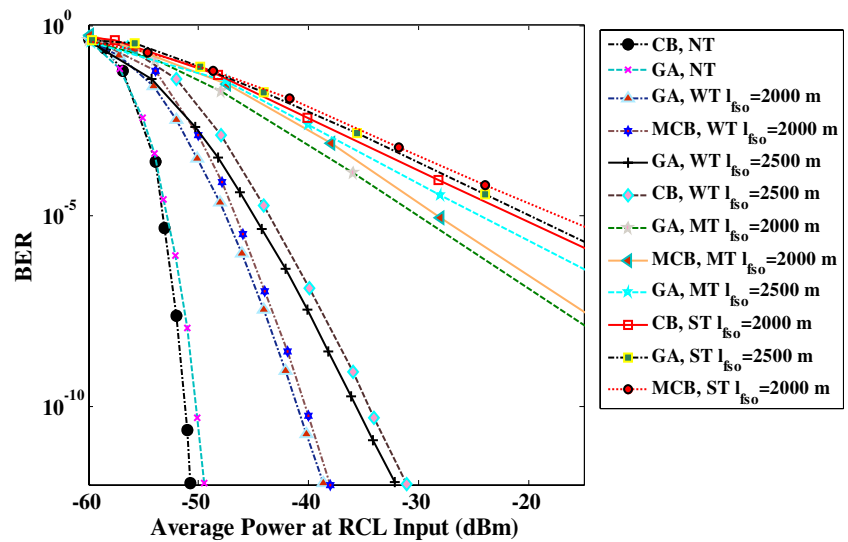


Fig. 12 MCB BER as a function of ATOP (dBm) for $\sigma_{PE}/\Gamma_{RX} = 0.2, 4 \text{ \& } 6$, $G = 30 \text{ dB}$, $M = 5$, for NT with GS, MT only with GS, no PE and combined (ST, MT, PE, and GS) with $D_{RX} = 50 \text{ mm}$

Fig. 13 BER vs. average power at RCL input (dBm) using the coding level $M=5$, $I_{\text{FSO}} = 2000$ m and 2500 m, $G=30$ dB, $D_{\text{Rx}} = 4$ mm for NT and ST, MT, WT [10, 25]



MT scenario with PE effects. In [65], the focus is on improving performance using an adaptive hybrid MQAM-MPPM scheme over Nakagami and log-normal dynamic visible light communication channels, addressing challenges such as ASE noise, atmospheric turbulence, pointing errors, and interchannel crosstalk. The paper explores the analysis and enhancement of the bit-error-rate performance using various techniques, considering challenges like ASE noise, atmospheric turbulence, pointing errors, and interchannel crosstalk. It discusses the use of M-ary hybrid DPPM-M-PAPM modulation schemes to enhance efficiency and reliability, along with the integration of adaptive optics to reduce turbulence effects and improve modulation efficiency. [65] emphasizes enhancing FSO communication efficiency through hybrid OOK modulation, M-ary DPPM, and M-PAPM in DWDM-FSO PON communication systems, considering factors such as ASE noise, atmospheric turbulence, pointing errors, and interchannel crosstalk. A comparison with [65] offers insights into different modulation approaches and system designs suitable for specific applications and operational conditions within optical communication systems. When evaluating the system model for various channel models, reference is made to the work conducted in [66] as a future endeavor. This provides insights into underwater visible light communication channel modeling.

Practical implications and applications

This section outlines potential applications in telecommunications, satellite communications, military operations, and optical wireless communications for urban development. The discussion focuses on the benefits of modulation techniques in these contexts, including improved data rate, enhanced signal integrity under atmospheric disturbances, and reduced

bit error rate, all critical for achieving robust and reliable communication. To demonstrate practical feasibility, a case study showcasing the simulation of M-ary Hybrid DPPM-M-PAPM modulation schemes using MATLAB is included. The study reflects performance enhancements in a DWDM-FSO PON system under conditions of atmospheric turbulence, ASE noise, and interchannel crosstalk. The results highlight improvements in optical signal-to-noise ratio and spectral efficiency, validating the effectiveness of the proposed schemes in controlled environments similar to real-world scenarios. Additionally, there is an acknowledgment of the necessity for robust system design and integration, with discussions on how these modulation techniques can be integrated into existing DWDM systems. This includes recommendations for modifications to transmitter and receiver designs, as well as adaptations in network infrastructure to support high-speed, efficient transmission capabilities provided by M-ary Hybrid DPPM-M-PAPM modulation. The practical applications and implications of these findings span various sectors:

- In real-world communication networks, enhancing telecommunication infrastructure, especially in urban areas, involves refining system architectures to boost reliability and efficiency during atmospheric disturbances and emergency response scenarios. The M-ary hybrid DPPM-M-PAPM modulation techniques can provide dependable connections under various atmospheric conditions.
- For satellite communications, enhanced modulation techniques improve the quality and throughput of data links between satellites and ground stations, essential for maintaining communication efficacy in adverse conditions [62–65].
- In military communications, secure and reliable channels are crucial for operations under diverse atmospheric

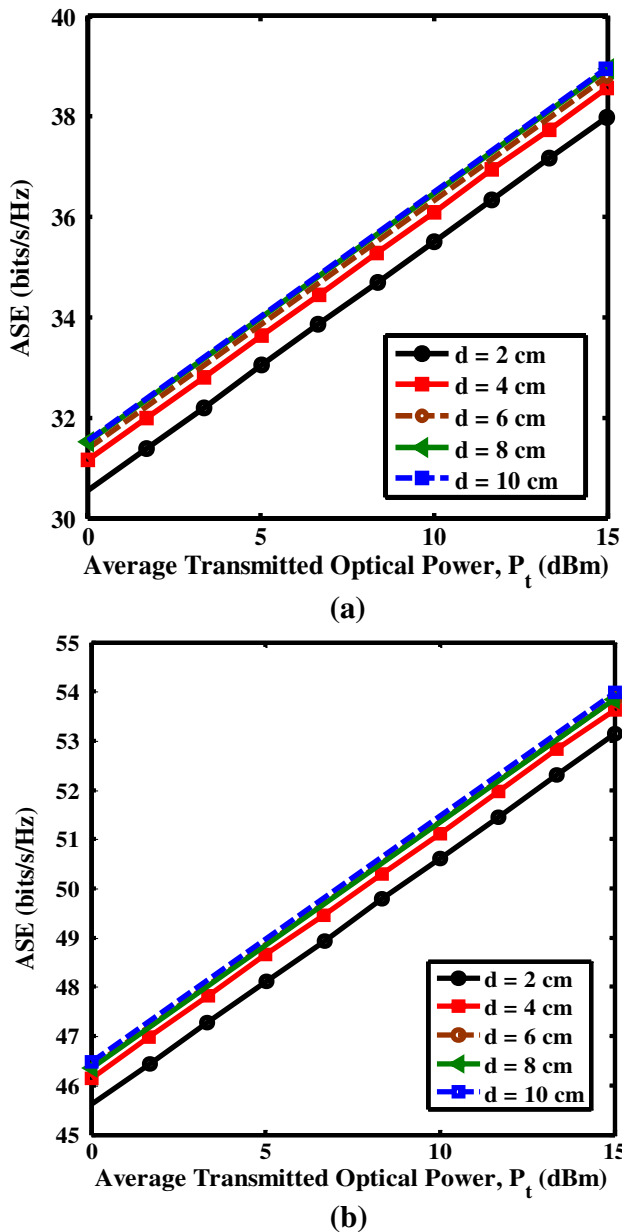


Fig. 14 The average spectral efficiency ASE (bits/s/Hz) is shown as a function of ATOP under ST (a) With PEs (b) Without PEs for M-ary hybrid M-PAPM-M-ary DPPM with AA and receiver aperture diameter d (cm) [10, 25]

conditions and potential electronic interference. The discussed modulation enhancements can significantly improve secure communication links.

- d. Integrating advanced FSO systems in smart cities facilitates efficient management of communication networks for various services.
- e. Enhancing communication systems within commercial aviation can significantly improve safety.
- f. Implementing M-ary DPPM-M-PAPM in existing DWDM systems may require hardware updates to

accommodate advanced modulation formats. Robustness and reliability tests are essential to confirm effectiveness under real-world conditions.

- g. Exploring practical applications of these modulation techniques enables effective utilization in communication systems and underwater optical wireless communications. The use of convolutional codes in dynamic underwater visible light communication systems and unmanned aerial vehicles (UAV) accounts for pointing errors and atmospheric turbulence [66–69].
- h. These enhancements substantially strengthen the manuscript, illustrating the practical impact and potential of the proposed modulation techniques. This expanded discussion aims to enrich the manuscript’s contribution to the field.

Conclusion and suggestions for future work

In this research, the exploration and enhancement of the HFFSO optical fiber communication network system involved incorporating a mix of modulation techniques, including OOK/M-ary DPPM-M-PAPM, within a DWDM-PON framework. Utilizing ICC methods for analysis, the performance of DWDM-DPPM systems was assessed in various scenarios like GA, CB, and MCB. The goal is to enhance spectral efficiency and mitigate crosstalk interferences within DWDM-PON/HFFSO configurations by integrating hybrid OOK/M-ary DPPM-M-PAPM modulation techniques, thereby improving overall reliability. Through theoretical BER evaluations, the efficacy of the OOK/M-ary hybrid DPPM modulation scheme has been showcased, particularly in turbulent atmospheric conditions. Findings suggest that the use of M-ary DPPM-M-PAPM modulation helps in minimizing ICC interferences and achieving superior BER performance. Moreover, the impact of turbulence on system performance has been studied, with a specific focus on M-ary DPPM-M-PAPM design versus OOK-NRZ, highlighting enhancements in power penalty and efficiency. The proposed architecture of M-ary DPPM-M-PAPM offers improved receiver sensitivity and reliability over OOK-NRZ. The study examines the comprehensive effects of aperture averaging on the average spectral efficiency of FSO links across turbulent channels with PEs. Implementing aperture averaging and reducing beam width positively impacts the average spectral efficiency performance in the presence of PEs. Future endeavors to enhance FSO DWDM optical fiber communication systems utilizing M-ary hybrid DPPM-M-PAPM modulation techniques will concentrate on experimental validation, optimizing adaptive optics, advanced signal processing analysis, optimizing multi-channel systems, and conducting real-world field trials to assess practical deployment viability. The future work for this study will involve conducting experimental validations to substantiate the efficacy of the proposed M-ary hybrid DPPM-M-PAPM modulation techniques in real-world FSO DWDM communication systems.

Additionally, it will explore the optimization of adaptive optics for dynamic system parameter adjustments in response to atmospheric turbulence, pointing errors, and interchannel crosstalk to enhance overall system performance. Further investigations will delve into advanced signal processing algorithms, error correction coding schemes, and multi-channel system optimizations to improve data transmission reliability, efficiency, and spectral utilization in FSO DWDM communication networks. The potential future work for the paper may involve exploring further optimization strategies for the proposed M-ary DPPM-M-PAPM modulation schemes to enhance system performance. This could include investigating adaptive coding techniques, advanced error correction coding, or signal processing algorithms to potentially improve overall efficiency and reliability of the communication system. Additionally, conducting practical experimentation or simulation studies to validate the theoretical findings and numerical results presented in the paper would be a valuable next step. This could help verify the feasibility and real-world applicability of the proposed hybrid modulation schemes under various environmental conditions and system parameters. Furthermore, considering the integration of emerging technologies such as machine learning, artificial intelligence, or deep learning algorithms in optimizing system design and performance could be an interesting avenue for future research. These technologies could offer novel solutions for addressing challenges like atmospheric turbulence, pointing errors, ASE noise, and interchannel crosstalk in communication systems. Exploring the application of the proposed hybrid OOK/M-ary DPPM-M-PAPM modulation schemes in other optical communication scenarios or networking architectures could also be a promising direction for communication systems and underwater optical wireless communications. The incorporation of convolutional codes in dynamic underwater visible light communication systems and UAVs addresses pointing errors and atmospheric turbulence for future work. This exploration may involve investigating the scalability, compatibility, and adaptability of the modulation techniques in various communication setups or network topologies to assess their broader impact and potential benefits.

Acknowledgements I sincerely thank the editor and reviewers for their diligent efforts in enhancing the manuscript. Their valuable contributions and commitment to excellence have greatly improved the quality and clarity of the work.

Funding This study did not receive any external funding.

Data availability The data that support the findings of this study are available within this article.

Declarations

Ethical approval Not applicable.

Conflict of interest The author declares no conflicts of interest.

References

1. A.J. Phillips, R.A. Cryan, J.M. Senior, An optically preamplified intersatellite PPM receiver employing maximum likelihood detection. *IEEE Photon. Technol. Lett.* **8**(5), 691–693 (1996). <https://doi.org/10.1109/68.491597>
2. A.O. Aladeloba, A.J. Phillips, M.S. Woolfson, Performance evaluation of optically preamplified digital pulse position modulation turbulent free-space optical communication systems. *IET Optoelectron.* **6**(1), 66–74 (2012). <https://doi.org/10.1049/iet-opt.2011.0029>
3. T. Ohtsuki, Performance analysis of indoor infrared wireless systems using PPM CDMA. *Electron. Commun. Japan, Part I Commun. (English Transl. Denshi Tsushin Gakkai Ronbunshi)* **85**(1), 1–10 (2002). <https://doi.org/10.1002/ecja.1062>
4. M.S. Leeson, Pulse position modulation for spectrum-sliced transmission. *IEEE Photon. Technol. Lett.* **16**(4), 1191–1193 (2004). <https://doi.org/10.1109/LPT.2004.824668>
5. A.M. Mbah, J.G. Walker, A.J. Phillips, Performance evaluation of turbulence-accentuated interchannel crosstalk for hybrid fibre and free-space optical wavelength-division-multiplexing systems using digital pulse-position modulation. *IET Optoelectron.* **10**(1), 11–20 (2016). <https://doi.org/10.1049/iet-opt.2015.0007>
6. I. Garrett, Pulse-position modulation for transmission over optical fibers with direct or heterodyne detection. *IEEE Trans. Commun.* **31**(4), 518–527 (1983). <https://doi.org/10.1109/TCOM.1983.1095842>
7. A.J. Phillips, R.A. Cryan, J.M. Senior, Optically preamplified pulse-position modulation for fibre-optic communication systems. *IEE Proc. Optoelectron.* **143**(2), 153–159 (1996). <https://doi.org/10.1049/ip-opt:19960180>
8. E.E. Elsayed, B.B. Yousif, M.M. Alzalabani, Performance enhancement of the power penalty in DWDM FSO communication using DPPM and OOK modulation. *Opt. Quant. Electron.* **50**(7), 282 (2018). <https://doi.org/10.1007/s11082-018-1508-y>
9. E.E. Elsayed, B.B. Yousif, Performance enhancement of M-ary pulse-position modulation for a wavelength division multiplexing free-space optical systems impaired by interchannel crosstalk, pointing error, and ASE noise. *Opt. Commun.* **475**, 126219 (2020). <https://doi.org/10.1016/j.optcom.2020.126219>
10. E.E. Elsayed, B.B. Yousif, Performance enhancement of the average spectral efficiency using an aperture averaging and spatial-coherence diversity based on the modified-PPM modulation for MISO FSO links. *Opt. Commun.* **463**, 125463 (2020). <https://doi.org/10.1016/j.optcom.2020.125463>
11. M. De Andrade, G. Kramer, L. Wosinska, J. Chen, S. Sallent, B. Mukherjee, Evaluating strategies for evolution of passive optical networks. *IEEE Commun. Mag.* **49**(7), 176–184 (2011). <https://doi.org/10.1109/MCOM.2011.5936171>
12. G. Kramer, G. Pesavento, Ethernet passive optical network (EPON): Building a next-generation optical access network. *IEEE Commun. Mag.* **40**(2), 66–73 (2002). <https://doi.org/10.1109/35.983910>
13. B. Kim, B.W. Kim, “WDM-PON development and deployment as a present optical access solution.” *Conf. Opt. Fiber Commun. Tech. Dig. Ser.* (2009). <https://doi.org/10.1364/ofc.2009.othp5>
14. K. Wang, A. Nirmalathas, C. Lim, E. Skafidas, 4 × 12.5 Gb/s WDM optical wireless communication system for indoor applications. *J. Light. Technol.* **29**(13), 1988–1996 (2011). <https://doi.org/10.1109/JLT.2011.2155622>
15. A.O. Aladeloba, M.S. Woolfson, A.J. Phillips, WDM FSO network with turbulence-accentuated interchannel crosstalk. *J. Opt. Commun. Netw.* **5**(6), 641–651 (2013). <https://doi.org/10.1364/JOCN.5.000641>
16. G.K. Chang et al., Key technologies of WDM-PON for future converged optical broadband access networks. *J. Opt. Commun. Netw.* **1**(4), C35 (2009). <https://doi.org/10.1364/JOCN.1.000C35>
17. B.B. Yousif, E.E. Elsayed, Performance enhancement of an orbital-angular-momentum-multiplexed free-space optical link

- under atmospheric turbulence effects using spatial-mode multiplexing and hybrid diversity based on adaptive MIMO equalization. *IEEE Access* 7, 84401–84412 (2019). <https://doi.org/10.1109/ACCESS.2019.2924531>
18. Y. Yamamoto, Noise and error rate performance of semiconductor laser amplifiers in PCM-IM optical transmission systems. *IEEE J. Quantum Electron.* **16**(10), 1073–1081 (1980). <https://doi.org/10.1109/JQE.1980.1070356>
 19. L.F.B. Ribeiro, J.R.F. Da Rocha, J.L. Pinto, Performance evaluation of EDFA preamplified receivers taking into account intersymbol interference. *J. Light. Technol.* **13**(2), 225–232 (1995). <https://doi.org/10.1109/50.365210>
 20. J.J. O'Reilly, J.R.F. Da Rocha, Improved error probability evaluation methods for direct detection optical communication systems. *IEEE Trans. Inf. Theory* **33**(6), 839–848 (1987). <https://doi.org/10.1109/TIT.1987.1057374>
 21. M.R. Hayal, B.B. Yousif, M.A. Azim, Performance enhancement of DWDM-FSO optical fiber communication systems based on hybrid modulation techniques under atmospheric turbulence channel. *Photonics* **8**, 464 (2021). <https://doi.org/10.3390/photonics8110464>
 22. A.A. Al-Orainy, J.J. O'Reilly, "Error probability bounds and approximations for the influence of crosstalk on wavelength division multiplexed systems." *IEE Proc. Part J, Optoelectron.* **137**(6), 379–384 (1990). <https://doi.org/10.1049/ip-j.1990.0066>
 23. S.D. Personick, Applications for quantum amplifiers in simple digital optical communication systems. *Bell Syst. Tech. J.* **52**(1), 117–133 (1973). <https://doi.org/10.1002/j.1538-7305.1973.tb03187.x>
 24. R. Ma, T.J. Zuo, S. Sujecki, A.J. Phillips, Improved performance evaluation for DC-coupled burst mode reception in the presence of amplified spontaneous emission noise and interchannel crosstalk. *IET Optoelectron.* **4**(3), 121–132 (2010). <https://doi.org/10.1049/iet-opt.2009.0007>
 25. E.E. Elsayed, B.B. Yousif, Performance enhancement of hybrid diversity for M-ary modified pulse-position modulation and spatial modulation of MIMO-FSO systems under the atmospheric turbulence effects with geometric spreading. *Opt. Quant. Electron.* **52**(12), 508 (2020). <https://doi.org/10.1007/s11082-020-02612-1>
 26. L.C. Andrews, R.L. Phillips, C.Y. Young, Laser beam scintillation with applications. *Laser Beam Scintill. with Appl.* (2009). <https://doi.org/10.1117/3.412858>
 27. P.V. Trinh, N.T. Dangy, T.C. Thang, A.T. Pham, Performance of all-optical amplify-and-forward WDM/fso relaying systems over atmospheric dispersive turbulence channels. *IEICE Trans. Commun.* **E99B**(6), 1255–1264 (2016). <https://doi.org/10.1587/transcom.2015EUP0004>
 28. A.K. Majumdar, Free-space laser communication performance in the atmospheric channel. *J. Opt. Fiber Commun. Reports* **2**(4), 345–396 (2005). <https://doi.org/10.1007/s10297-005-0054-0>
 29. M.A. Khalighi, N. Schwartz, N. Aitamer, S. Bourennane, Fading reduction by aperture averaging and spatial diversity in optical wireless systems. *J. Opt. Commun. Netw.* **1**(6), 580–593 (2009). <https://doi.org/10.1364/JOCN.1.000580>
 30. M.A. Al-Habash, Mathematical model for the irradiance probability density function of a laser beam propagating through turbulent media. *Opt. Eng.* **40**(8), 1554 (2001). <https://doi.org/10.1117/1.1386641>
 31. W.O. Popoola, Z. Ghassemlooy, BPSK subcarrier intensity modulated free-space optical communications in atmospheric turbulence. *J. Light. Technol.* **27**(8), 967–973 (2009). <https://doi.org/10.1109/JLT.2008.2004950>
 32. K.N.S. Rajiv Ramaswami, "Optical networks a practical perspective," San Francisco, CA Morgan Kaufmann (3), 1–857, 2010, [Online]. <http://www.cesarkallas.net/arquivos/faculdade-pos/TP319-redes-opticas/Optical-Networks-3nd.pdf>. Accessed 2010
 33. K. Maru, T. Mizumoto, H. Uetsuka, Demonstration of flat-pass-band multi/demultiplexer using multi-input arrayed waveguide grating combined with cascaded Mach-Zehnder interferometers. *J. Light. Technol.* **25**(8), 2187–2197 (2007). <https://doi.org/10.1109/JLT.2007.901339>
 34. A. Hirano, Y. Miyamoto, S. Kuwahara, "Performances of CSRZ-DPSK and RZ-DPSK in 43-Gbit/s/ch DWDM G.652 single-mode-fiber transmission." *Conf. Opt. Fiber Commun. Tech. Dig. Ser.* **86**, 454–456 (2003). <https://doi.org/10.1109/ofc.2003.315949>
 35. C.X. Yu, D.T. Neilson, Diffraction-grating-based (de)multiplexer using image plane transformations. *IEEE J. Sel. Top. Quantum Electron.* **8**(6), 1194–1201 (2002). <https://doi.org/10.1109/JSTQE.2002.805977>
 36. P.S. Henry, "Error-rate performance of optical amplifiers," 170 (1989). <https://doi.org/10.1364/ofc.1989.thk3>
 37. E.E. Elsayed, B.B. Yousif, Performance evaluation and enhancement of the modified OOK based IM/DD techniques for hybrid fiber/FSO communication over WDM-PON systems. *Opt. Quant. Electron.* **52**(9), 385 (2020). <https://doi.org/10.1007/s11082-020-02497-0>
 38. A.M. Mbah, J.G. Walker, A.J. Phillips, Performance evaluation of digital pulse position modulation for wavelength division multiplexing FSO systems impaired by interchannel crosstalk. *IET Optoelectron.* **8**(6), 245–255 (2014). <https://doi.org/10.1049/iet-opt.2013.0145>
 39. B.B. Yousif, E.E. Elsayed, M.M. Alzalabani, Atmospheric turbulence mitigation using spatial mode multiplexing and modified pulse position modulation in hybrid RF/FSO orbital-angular-momentum multiplexed based on MIMO wireless communications system. *Opt. Commun.* **436**, 197–208 (2019). <https://doi.org/10.1016/j.optcom.2018.12.034>
 40. A.M. Mbah, J.G. Walker, A.J. Phillips, Outage probability of WDM free-space optical systems affected by turbulence-accentuated interchannel crosstalk. *IET Optoelectron.* **11**(3), 91–97 (2017). <https://doi.org/10.1049/iet-opt.2016.0057>
 41. A.O. Aladeloba, A.J. Phillips, M.S. Woolfson, Improved bit error rate evaluation for optically pre-amplified free-space optical communication systems in turbulent atmosphere. *IET Optoelectron.* **6**(1), 26–33 (2012). <https://doi.org/10.1049/iet-opt.2010.0100>
 42. A.O. Aladeloba, A.J. Phillips, M.S. Woolfson, DPPM FSO communication systems impaired by turbulence, pointing error and ASE noise. *Int. Conf. Transparent Opt. Netw.* (2012). <https://doi.org/10.1109/ICTON.2012.6253854>
 43. B. Mukherjee, WDM optical communication networks: progress and challenges. *IEEE J. Sel. Areas Commun.* **18**(10), 1810–1824 (2000). <https://doi.org/10.1109/49.887904>
 44. K. Mallick, P. Mandal, G.C. Mandal, R. Mukherjee, B. Das, A.S. Patra, Hybrid MMW-over fiber/OFDM-FSO transmission system based on doublet lens scheme and POLMUX technique. *Opt. Fiber Technol.* **52**, 101942 (2019). <https://doi.org/10.1016/j.yofte.2019.101942>
 45. K. Mallick, P. Mandal, R. Mukherjee, G.C. Mandal, B. Das, A.S. Patra, Generation of 40 GHz/80 GHz OFDM based MMW source and the OFDM-FSO transport system based on special fine tracking technology. *Opt. Fiber Technol.* **54**, 102130 (2020). <https://doi.org/10.1016/j.yofte.2019.102130>
 46. S. Idris, H. Selmy, W.T.A. Lopes, Performance analysis of hybrid MPAPM technique for deep-space optical communications. *IET Commun.* **15**(13), 1700–1709 (2021). <https://doi.org/10.1049/cmu2.12182>
 47. S. Magidi, A. Jabeena, Analysis of multi-pulse position modulation free space optical communication system employing wavelength and time diversity over Malaga turbulence channel. *Sci. African* **12**, e00777 (2021). <https://doi.org/10.1016/j.sciaf.2021.e00777>
 48. A. Alipour, A. Farmani, A. Mir, Analysis of optical power budget in DWDM-FSO link under outdoor atmospheric channel model. *Opt. Quant. Electron.* **53**(8), 446 (2021). <https://doi.org/10.1007/s11082-021-03112-6>
 49. H. Ran, J. Zhang, G. Pan, Y. Xie, Outage probability of wireless-powered multi-relaying MIMO FSO-RF systems. *Opt. Commun.* **498**, 127260 (2021). <https://doi.org/10.1016/j.optcom.2021.127260>

50. T. Zhang, P. Wang, T. Liu, C. Jia, W. na Pang, W. Wang, Performance analysis of multi-hop parallel FSO system over double generalized gamma distribution considering two transmission beams. *Optoelectron. Lett.* **17**(4), 215–220 (2021). <https://doi.org/10.1007/s11801-021-0093-7>
51. A.E. Willner et al., Perspectives on advances in high-capacity, free-space communications using multiplexing of orbital-angular-momentum beams. *APL Photonics* **6**(3), 030901 (2021). <https://doi.org/10.1063/5.0031230>
52. K. Sharma, S.K. Grewal, Performance assessment of hybrid PPM–BPSK–SIM based FSO communication system using time and wavelength diversity under variant atmospheric turbulence. *Opt. Quant. Electron.* **52**(10), 430 (2020). <https://doi.org/10.1007/s11082-020-02547-7>
53. M. Singh, J. Malhotra, Performance comparison of M-QAM and DQPSK modulation schemes in a 2×20 Gbit/s–40 GHz hybrid MDM–OFDM-based radio over FSO transmission system. *Photonic Netw. Commun.* **38**(3), 378–389 (2019). <https://doi.org/10.1007/s11107-019-00861-z>
54. S. Malik, P.K. Sahu, Performance analysis of free space optical communication system using different modulation schemes over weak to strong atmospheric turbulence channels. *Lect. Notes Electr. Eng.* **546**, 387–399 (2020). https://doi.org/10.1007/978-981-13-6159-3_41
55. V. Srivastava, A. Mandloi, G.G. Soni, Outage probability and average BER estimation of FSO system employing wavelength diversity. *Opt. Quant. Electron.* **51**(7), 229 (2019). <https://doi.org/10.1007/s11082-019-1943-4>
56. R. Mukherjee et al., PAM-4 based long-range free-space-optics communication system with self-injection locked QD-LD and RS codec. *Opt. Commun.* **476**, 126304 (2020). <https://doi.org/10.1016/j.optcom.2020.126304>
57. R. Mukherjee, K. Mallick, P. Mandal, B. Dutta, B. Kuiri, A.S. Patra, Bidirectional hybrid OFDM based free-space/wireless-over-fiber transport system. *Opt. Quant. Electron.* **52**(6), 311 (2020). <https://doi.org/10.1007/s11082-020-02428-z>
58. P. Saxena, A. Mathur, M.R. Bhatnagar, BER performance of an optically pre-amplified FSO system under turbulence and pointing errors with ASE noise. *J. Opt. Commun. Netw.* **9**(6), 498–510 (2017). <https://doi.org/10.1364/JOCN.9.000498>
59. E.E. Elsayed, A.G. Alharbi, M. Singh, A. Grover, Investigations on wavelength-division multiplexed fibre/FSO PON system employing DPPM scheme. *Opt. Quant. Electron.* **54**(6), 358 (2022). <https://doi.org/10.1007/s11082-022-03717-5>
60. E.E. Elsayed, D. Kakati, M. Singh et al., Design and analysis of a dense wavelength-division multiplexed integrated PON-FSO system using modified OOK/DPPM modulation schemes over atmospheric turbulences. *Opt. Quant. Electron.* **54**, 768 (2022). <https://doi.org/10.1007/s11082-022-04142-4>
61. E.E. Elsayed, Atmospheric turbulence mitigation of MIMO-RF/FSO DWDM communication systems using advanced diversity multiplexing with hybrid N-SM/OMI M-ary spatial pulse-position modulation schemes. *Opt. Commun.* **562**, 130558 (2024). <https://doi.org/10.1016/j.optcom.2024.130558>
62. M. Singh, E.E. Elsayed, M. Alayedi et al., Performance analysis in spectral-amplitude-coding-optical-code-division-multiple-access using identity column shift matrix code in free space optical transmission systems. *Opt. Quant. Electron.* **56**, 795 (2024). <https://doi.org/10.1007/s11082-023-05721-9>
63. G. Aarthi, K. Prabu, G.R. Reddy, Aperture averaging effects on the average spectral efficiency of FSO links over turbulence channel with pointing errors. *Opt. Commun.* **385**, 136–142 (2017). <https://doi.org/10.1016/j.optcom.2016.10.041>
64. E.E. Elsayed, B.B. Yousif, M. Singh, Performance enhancement of hybrid fiber wavelength division multiplexing passive optical network FSO systems using M-ary DPPM techniques under inter-channel crosstalk and atmospheric turbulence. *Opt. Quant. Electron.* **54**, 116 (2022). <https://doi.org/10.1007/s11082-021-03485-8>
65. A.E.A. El-Fikky, A.S. Ghazy, H.S. Khallaf, E.M. Mohamed, H.M.H. Shalaby, M.H. Aly, On the performance of adaptive hybrid MQAM–MPPM scheme over Nakagami and log-normal dynamic visible light communication channels. *Appl. Opt.* **59**, 1896–1906 (2020)
66. M. Mahmoud, A.I. Boghdady, A.E.-R.A. El-Fikky, M.H. Aly, Statistical studies using goodness-of-fit techniques with dynamic underwater visible light communication channel modeling. *IEEE Access* **9**, 57716–57725 (2021). <https://doi.org/10.1109/ACCESS.2021.3072689>
67. A. Elfikky, Z. Rezki, Symbol detection and channel estimation for space optical communications using neural network and autoencoder. *IEEE Trans. Mach. Learn. Commun. Netw.* **2**, 110–128 (2024). <https://doi.org/10.1109/TMLCN.2023.3346811>
68. A. Elfikky, A.I. Boghdady, A.G. AbdElkader et al., Performance analysis of convolutional codes in dynamic underwater visible light communication systems. *Opt. Quant. Electron.* **56**, 55 (2024). <https://doi.org/10.1007/s11082-023-05325-3>
69. M.R. Hayal, E.E. Elsayed, D. Kakati et al., Modeling and investigation on the performance enhancement of hovering UAV-based FSO relay optical wireless communication systems under pointing errors and atmospheric turbulence effects. *Opt. Quant. Electron.* **55**, 625 (2023). <https://doi.org/10.1007/s11082-023-04772-2>

Publisher’s Note Springer Nature remains neutral with regard to jurisdictional claims in published maps and institutional affiliations.

Springer Nature or its licensor (e.g. a society or other partner) holds exclusive rights to this article under a publishing agreement with the author(s) or other rightsholder(s); author self-archiving of the accepted manuscript version of this article is solely governed by the terms of such publishing agreement and applicable law.



Ebrahim E. Elsayed